Available online at www.sciencedirect.com
ScienceDirect
Journal of the European Ceramic Society 29 (2009) 419–424
www.elsevier.com/locate/jeurceramsoc

Dielectric loss caused by oxygen vacancies in titania ceramics

Robert C. Pullar [a,*], Stuart J. Penn [a], Xiaoru Wang [a], Ian M. Reaney [b], Neil McN. Alford [a]

[a] Department of Materials, Imperial College London, Exhibition Road, London SW7 2AZ, UK
[b] Department of Engineering Materials, University of Sheffield, Mappin Street, Sheffield S1 3JD, UK

Received 6 June 2008; accepted 23 June 2008

Abstract

Undoped TiO_2 exhibited deterioration in microwave (MW) dielectric loss as it reached its maximum density due to the reduction of Ti^{4+} to Ti^{3+} causing oxygen vacancies at high sintering temperatures. By adding small amounts of acceptor dopants with ionic radii between 0.5 and 0.95 Å, reduction during sintering was suppressed. The upper limit of ionic radius was discrete with almost no observed effect using dopants >0.96 Å ionic radius. In addition, the microwave dielectric loss of undoped TiO_2 could be improved by annealing at 1500 °C for 10 h in air, presumably as a result of re-oxidation. High loss samples exhibited a dark 'core' to the naked eye which was absent in low loss ceramics. Transmission electron microscopy revealed that grains in the dark core contained planar defects attributed to the condensation of O vacancies onto specific crystallographic planes, in a manner similar to that observed in Magnelli phases.

Keywords: Oxygen deficiency; Defects; Electron microscopy; Dielectric properties; TiO_2

1. Introduction

TiO_2 possesses a relative permittivity (ε') which is highly anisotropic in single crystals, $\varepsilon' = 89$ and 173 perpendicular and parallel to the *c*-axis, respectively,[1] but which averages to 100 in randomly oriented polycrystalline samples. Strong temperature dependence of the dielectric constant results in a high temperature coefficient of resonant frequency ($\tau_f \sim 450\,ppm\,K^{-1}$) and although microwave filters have been constructed using TiO_2,[2,3] it is generally considered to be unsuitable for this reason. Instead, TiO_2 is found as a constituent raw material in many temperature stable dielectric resonator (DR) compositions, e.g. Ba–Ti–O, Ba–RE–Ti–O (RE = Rare Earth), Zr–Sn–Ti–O (ZST), in composites with Al_2O_3, and doped $CaTiO_3$. One problem of utilising TiO_2 as a raw material is that the Ti ion can exist in several valence states. This may lead to the presence of O vacancies ($V_O^{\bullet\bullet}$) which are considered detrimental to the dielectric loss (tan δ), often expressed as a quality factor, Q, where $Q = 1/\tan\delta$.

Typically in TiO_2-based ceramics such as $BaTiO_3$,[4] "coring" is observed; a term used to describe the dark, oxygen deficient interior of a sintered pellet. In order to combat oxygen loss in the capacitor industry, $BaTiO_3$ is modified with acceptor dopants such as Mn which inhibit the formation of Ti^{3+}[5] in accordance with the defect equation,

$$Mn^{3+} + Ti^{3+} \rightarrow Mn^{2+} + Ti^{4+}.$$

In rutile reduced in H_2 to form $TiO_{1.8}$ (Ti_5O_9 with <1% Ti_6O_{11}/Ti_4O_7), $V_O^{\bullet\bullet}$ condense onto specific crystallographic planes which ultimately shear to create new structures, generically referred to as Magnelli phases.[6,7] The space charge potential and the spatial distributions of defects in TiO_2 have been calculated and shown to vary with donor or acceptor doping.[8] In addition, Templeton et al.[9] showed that dense, high purity TiO_2 had a high dielectric loss, $Q_f < 6000$ GHz ($Q_f = Q^*$ resonant frequency in GHz). Furthermore, they demonstrated that doping with a range of divalent and trivalent acceptor cations with ionic radii between 0.5 and 0.95 Å greatly decreased dielectric loss, while other cations had little or no effect.[9] The low Q_f associated with undoped TiO_2 was attributed to the presence of Ti^{3+} and, as a consequence, $V_O^{\bullet\bullet}$, whereas the improvement in Q in doped TiO_2 was considered to arise from a similar charge compensation mechanism to that shown above.

In this paper, the authors report the effect of 16 further cation dopants in TiO_2 which are compared with those reported previously.[9] The effects of sintering time and annealing were

* Corresponding author. Tel.: +44 207 815 7540; fax: +44 207 815 7599.
E-mail address: r.pullar@imperial.ac.uk (R.C. Pullar).

0955-2219/$ – see front matter © 2008 Elsevier Ltd. All rights reserved.
doi:10.1016/j.jeurceramsoc.2008.06.019

also investigated and the cores of doped and undoped TiO_2 were studied using transmission electron microscopy.

2. Experimental

2.1. Sample preparation

Doped samples were prepared by adding 0.05 mol% of the dopant to TiO_2 (PiKem Ltd., UK—purity details given in Section 3) as a dry powder, and then mixing by dry milling for 12 h using a teflon pot containing Y stabilised zirconia (YSZ) balls. The raw materials used for the dopants were either oxides or carbonates in the case of Na, K, Ba, Sr and Ca dopants, with purities of 99.9% or greater with the exception of Ag which was added as a pure metal flake. Cr was added as both Cr^{3+} (Cr_2O_3) and Cr^{6+} (CrO_3). Co was added as both CoO and Co_3O_4. The use of YSZ media ensured that contamination from the milling process was kept to a minimum.[9] Samples were uniaxially pressed to form green pellets, under a pressure of 100 MPa using a 13-mm diameter die. Sufficient powder was used to give a puck that would be approximately 4 mm high after sintering. The pucks were then sintered 1 h in air at 1500 °C, using a ramping and cooling rate of 5 °C min^{-1} unless otherwise stated.

2.2. Physical characterisation

The surface areas were measured on a Surface Area Analyser (Coulter SA3100), using N_2 as the adsorption gas, and samples were degassed at 300 °C for 2 h prior to analysis. The surface areas were calculated from adsorption/desorption isotherms using the BET method, and the equivalent spherical diameter was estimated. Grain sizes were measured from SEM micrographs (Hitachi S-4300) using the linear intercept method. No adjustment was made for the grain shape.[10]

2.3. Microwave measurements

The quality factor (Q) and relative permittivity (ε_r) were measured at room temperature on as fired ceramics at ~3 GHz, using the resonant $TE_{01\delta}$ mode of the sample.[11] The sample was placed in an oxygen-free high-conductivity copper cavity, supported on a 4-mm high low-loss quartz spacer. The cavity was 30 mm in diameter, with adjustable height. This height was adjusted so that the space above and below the sample was 4 mm, approximately the same as the sample thickness. The diameter of the sample was also approximately 1/3 of the diameter of the cavity, as recommended by Kajfez and Guillon.[11] The surface resistance of the copper was calculated from the Q value of the TE_{011} resonance of the empty cavity, to allow the results to be corrected for any loss due to the cavity walls.[11] The $TE_{01\delta}$ mode was examined using a Vector Network Analyser (Hewlett-Packard HP8720D), with a resolution of one Hz. The Q values are corrected for losses due to the measurement equipment, and so can be assumed to be the Q of the dielectric ceramic.

τ_f was obtained by continuously measuring the variation in resonant frequency (f_r) of the sample between 250 and 310 K using a heating and cooling at a rate of 2 °C min^{-1}. The results are quoted in ppm of f_r per degree K, at room temperature (e.g., 1 ppm of 7 GHz = 7 kHz). The samples were cooled by placing the cavity in a closed-cycle cooling system using a refrigerator (CTI Cryogenics Model 22) and cryocompressor (CTI Cryogenics model 8200). The temperature was controlled and measured using a Temperature Controller (Lakeshore 330) and in-house software.

2.4. Transmission electron microscopy (TEM)

Samples were prepared for transmission electron microscopy (TEM) by grinding pellets to a thickness of ~30 μm. These were affixed to copper rings and milled to perforation at an incidence angle of 15° using a Gatan duo ion mill (600 model). TEM was performed on an FEI Tecnai 20 operating at 200 kV.

3. Results and discussion

Undoped TiO_2 powder (PiKem, UK) had a range of impurities measured at 50 ppm Sn, 10 ppm Si, 3 ppm Ag, 3 ppm B and <1 ppm Mg.[9] Sintering at 1500 °C was required to achieve densities >98% theoretical. However by varying sintering temperature between 1400 °C and 1500 °C, the density could be controlled systematically. As density increased to ~94% of the theoretical value, Q_f steadily increased up to ~25 000 GHz but with a further increase in density to a maximum of 97%, Q_f deteriorated to ~6000 GHz.[9] Rutile is slightly oxygen deficient at these temperatures,[6] and although the samples appeared a uniformly pale greyish-yellow on the surface, when polished a darker core was revealed, with a pale greyish-yellow ring around the edge (Fig. 1a). Such coring effects have been reported in ZST,[12] and it has been shown that in $BaTi_4O_9$ and $Ba_2Ti_9O_{20}$ ceramics low concentrations of lattice defects, caused by reduction, degrade Q to almost zero.[4] Consequently, acceptor doping with Mn oxide is often used to ensure optimum MW properties.[5] The following sections report the results of an extensive study in TiO_2 aimed at understanding the role of dopants in optimising Q.

3.1. Doped TiO_2 samples

Dopants for TiO_2 were all added at 0.05 mol% and chosen with a range of valence states and ionic radii (from Shannon[13]), listed in Table 1 along with Q_f values (at 3 GHz) of the resulting ceramic and a visual assessment of their colour. All ceramics had densities >95% of the theoretical density of TiO_2 except those doped with Pb (93.2%) and Bi (94.3%). Consequently, ε_r values

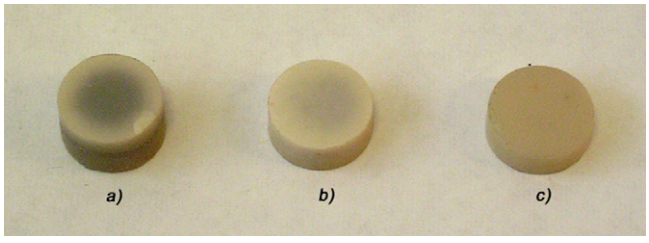

Fig. 1. Photograph showing evidence of coring in some samples: (a) Pure TiO_2, (b) 0.05 mol% Sm^{3+} doped TiO_2 and (c) 0.05 mol% Al^{3+} doped TiO_2 (no coring).

Table 1
Ionic radii (from Shannon[13]) and Q_f (at 3 GHz) for 0.05 mol% doped TiO_2

Dopant (0.05 mol%)	Valency	Ionic radius (Å)	Q_f (GHz)	Colour
Pure TiO_2	n/a	Ti^{4+} = 0.605	<6 000	Greyish-yellow, coring
Na	1+	1.02	8 400	Pale greyish-yellow
K	1+	1.38	8 100	Pale greyish-yellow
Ag	1+	1.15	4 478	Greyish-yellow, coring
Mg	2+	0.72	30 000	Pale grey
Ca	2+	1.06	0	Pale grey
Sr	2+	1.18	0	Pale greyish-yellow, coring
Ba	2+	1.35	0	Greyish-yellow, coring
Mn	2+	0.67 (low spin)	48 000	Brown
Co	2+	0.65 (low spin)	44 841	Dark Tan
Ni	2+	0.69	41 965	Light brown
Cu	2+	0.73	48 000	Dark greyish-yellow
Zn	2+	0.74	48 900	Dark greyish-yellow
Pb	2+	1.19	13 142	Pale greyish-yellow
B	3+	0.27	0	Grey-yellow, coring
Al	3+	0.535	47 100	Pale greyish-yellow
Cr	3+	0.615	46 326	Dark greyish brown
Fe	3+	0.55 (low spin)	50 100	Pale Yellow
Y	3+	0.90	36 000	Pale greyish-yellow
La	3+	1.032	0	Pale grey
Pr	3+	0.99	6 610	Dark grey surface, yellowish interior
Nd	3+	0.983	0	Patchy grey surface, yellowish interior
Sm	3+	0.958	0	Pale greyish-yellow, coring
Gd	3+	0.938	20 559	Pale greyish-yellow
Dy	3+	0.912	24 291	Pale greyish-yellow
Er	3+	0.89	33 428	Pale greyish-yellow
Bi	3+	1.03	15 950	Pale greyish-yellow
Si	4+	0.40	0	Metallic grey
Zr	4+	0.72	0	Greyish-yellow, coring
Sn	4+	0.69	0	Greyish-yellow, coring
Ce	4+	0.87	3 615	Patchy grey surface, yellowish interior
V	5+	0.54	30 861	Dark brown
Nb	5+	0.64	0	Dark grey
Ta	5+	0.64	0	Pale grey
Cr	6+	0.44	38 167	Dark greyish brown
Mo	6+	0.59	25 703	Blotchy dark grey
W	6+	0.60	0	Blotchy dark grey

were consistently ~100, except for the Pb and Bi doped samples with lower density for which $\varepsilon_r = 87.3$ and 93.1, respectively. Samples with $Q_f = 0$ had no detectable resonant peak and Q values of samples previously published but remeasured for this study results were in close agreement with the new data.[9]

The Q_f is plotted against ionic radius in Fig. 2 in which samples split roughly into two groups. The first exhibits $Q_f > 20\,000$ GHz with ionic radii between 0.5 and 0.95 Å. The second group possess ionic radii outside these limits and generally $Q_f \ll 20\,000$ GHz. Nearly all of the samples with high (>20 000 GHz) Q_f values have valence state of 3+ or 2+ with the exception of Cr^{6+}, V^{5+} and Mo^{6+}.

Although Cr^{6+} was present in the raw oxide (CrO_3) when added as a dopant to TiO_2, it is unlikely that this oxidation state is maintained during sintering. It is anticipated that Cr^{6+} would reduce to either Cr^{4+}, Cr^{3+}or Cr^{2+}, increasing the ionic radius to within the ideal 0.5–0.95 Å range. Typically minor impurities of CrO_3, Cr_2O_3 and CrO in essentially colourless matrices such as TiO_2, induce reddish-purple, green and black hues, respectively. The black colour of both pucks doped with Cr-oxide

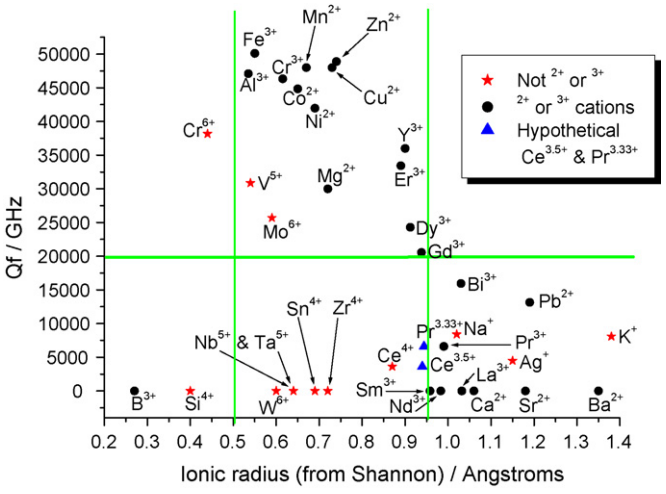

Fig. 2. Plot of Q_f against six co-ordinate ionic radius[13] for doped TiO_2. The green lines indicate the limits of the ideal range for ionic radius of a dopant to obtain high Q.

suggests that Cr^{2+} cations may be present irrespective of the initial valence state of the raw material. Similarly, V^{5+} may also have been reduced to a lower oxidation state ensuring that sintering pucks contain dopant V ions within the experimentally determined ideal 0.5–0.95 Å range. In contrast, Mo^{6+} is a very stable oxidation state and not expected to reduce even at the sintering temperatures suggested. Both Mo^{6+} and W^{6+} doped samples exhibited an inhomogeneous distribution of colour.

Not withstanding the unexplained behaviour of Mo^{6+}, the general trend that acceptor dopants with ionic radii between 0.5 and 0.95 Å give high Q_f values is self-evident in the data. In particular, Al^{3+} and the first row transition metals Fe^{3+}, Mn^{2+}, Zn^{2+}, Cu^{2+}, Cr^{3+}, Co^{2+} Ni^{2+} exhibit $Q_f > 40\,000$ GHz and all have ionic radii similar to Ti^{4+} (0.605 Å). For samples doped with stable 4+ and 5+ ions, coring was often observed and such samples exhibited high losses. This suggests that even though most of them have the correct ionic radius, they do not inhibit reduction of Ti^{4+}. In the case of 5+ ions they are more likely to act as donors of electrons, resulting in increased dielectric loss and conduction,[14–16] e.g., Nb-doped TiO_2 which is used as an oxygen sensor.[17]

The group of dopants B_2O_3 (B^{3+}), Bi_2O_3 (Bi^{3+}) and PbO (Pb^{2+}) are low melting point oxides, additionally SiO_2 when reacted with network modifiers forms low melting point glass phases. Consequently, these oxides may be used as sintering aids, forming liquid phase at the grain boundary during sintering. Often such phases, although lower in Q than the matrix act as short circuit diffusion paths for O diffusion, inhibiting reduction by allowing the rapid ingress of O on cooling. This may account for their positive effect on Q with respect to undoped TiO_2. The larger 2+ cations all had large losses, but 1+ cations, whilst still having large radii, had measurable Q values, although still poor for dielectric resonators.

The rare earth metals are especially interesting, as their ionic radii cross-over the 0.95 Å border, and most have a valency of 3+. The ionic radii of the rare earth ions increase systematically with Er^{3+} the smallest (0.89 Å) increasing to the largest, $La^{3+} = 1.03$ Å in six fold coordination. Between Gd^{3+} (0.94 Å) and Sm^{3+} (0.96 Å) there is an anomalous decrease in Q from >20 000 to an unmeasurable value (Fig. 3). Pr^{3+} and Ce^{4+} are exceptions but cerium ions are known to exhibit variable valence states[18,19] with 3+ favoured under reducing conditions. This leads to an increase in average ionic radius and thus Ce ions may be considered to have a larger ionic radius than nominally quoted for the 4+ state. Similarly, the oxidation state of the Pr ions is imprecise with higher valences possible than that nominally added (Pr_2O_3, 3+).[20] Although Pr^{3+} was added as the pale green Pr_2O_3, the preferred oxide of praseodymium is often the black coloured Pr_6O_{11}, when heated in air. However, Pr_6O_{11} is often reduced to Pr_2O_3 by any oxygen deficiency,[20] such as Ti^{3+} cations. It is therefore likely that the oxidation state is some where between these values—mixed Pr_xO_y films consisting of both Pr_2O_3 and Pr_6O_{11} have been reported.[21] Moreover, the Pr^{3+} doped sample was black on the surface, but pale greyish-yellow on the underside and interior, suggesting that the dopant has been oxidised to higher valence only where exposed to air.

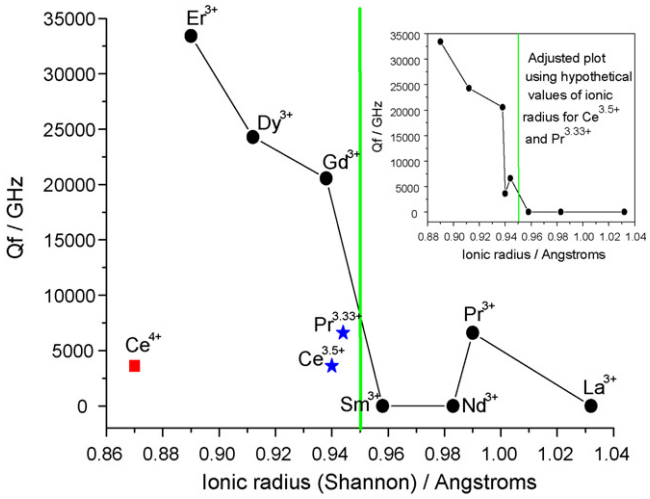

Fig. 3. Plot of Q_f against ionic radius for rare earth metal dopants. The stars indicate the positions of hypothetical $Ce^{3.5+}$ and $Pr^{3.33+}$ cations, and these are incorporated into the plot in the small insert.

Therefore, we added two hypothetical cations to Fig. 3, with arbitrary values in the middle of these possible ranges of oxidation state; that is $Ce^{3.5+}$ (Ce_2O_7) and $Pr^{3.33+}$ (Pr_3O_5). Using the six co-ordinate ionic radii of Ce^{3+} (1.01 Å) and Pr^{4+} (0.85 Å),[13] hypothetical values were estimated for $Ce^{3.5+}$ (0.940 Å) and $Pr^{3.33+}$ (0.944 Å), which put them just inside the 0.95 Å border, their relatively low Q_f values maybe reflecting their closeness to this limit (see insert, Fig. 3). *It must be stressed that these values are merely indications of how these cations may fit within the apparently precise cut-off point of 0.95 Å, and we are not suggesting that these are the exact oxidation states of these cations.*

It can therefore be suggested that, in the absence of secondary phases, high Q TiO_2 ceramics will be formed under the following conditions:

1. The valency must be <4+, to favour stabilisation of Ti^{4+} with the best dopants having 2+ and 3+ oxidation states.
2. The dopant cation has an ionic radius between 0.5 and 0.95 Å ($Ti^{4+} = 0.605$ Å), with a very precise cut off point at 0.95 Å, above which low Q TiO_2 ceramics occur.
3. The exception to this seems to be 1+ ions, which give lower-but-measurable Q values despite their larger ionic radius.

3.2. *Effects of sintering time and annealing on microstructure and dielectric loss*

Previous studies of dense alumina have shown that grain size has an important influence upon Q.[22] No such studies could be made of high purity titania, as oxygen deficiency within the core resulted in high dielectric losses. Undoped and doped PiKem TiO_2 samples, sintered for 2 h, were studied by SEM to determine if the dopants influenced grain size, and if this correlated

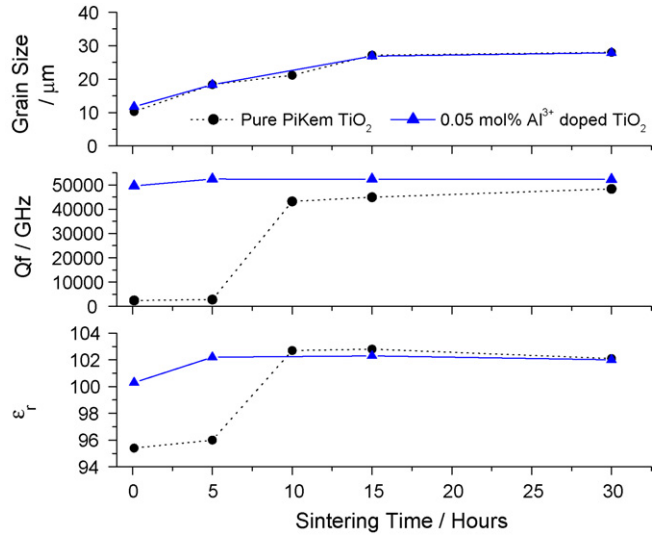

Fig. 4. Effect of sintering time on grain growth and dielectric properties. The samples were sintered at 1500 °C, for between 10 min and 30 h.

to improvements in Q. No relationship was found between grain size and Q values in the doped TiO_2 samples, and many high Q doped samples had microstructures resembling pure TiO_2 samples. Therefore, the effects of differing sintering times were studied. The samples were sintered for between 0.1 and 30 h, at 1500 °C. The heating and cooling rates were 5 °C min^{-1} for all samples. All samples, even those sintered for only 0.1 h, had densities >98%, and the results are shown in Fig. 4. Grain growth occurred largely in the first 15 h of sintering, with longer times resulting in only a nominal increase in grain size. It is evident that the undoped and doped samples have almost identical grain growth, demonstrating that grain size and distribution does not account for the differences in Q_f. In addition, for sintering times >10 h, undoped PiKem TiO_2 underwent a large increase in Q, approaching that of the Al^{3+} doped samples irrespective of the absence of grain growth. The colour of pure TiO_2 samples with high Q was uniform pale greyish-yellow with no coring, but the samples with very poor Q values repeatedly exhibited dark cores.

The precise value of ε_r is related to density in dielectric ceramics. However, a small increase in ε_r to a maximum of 102 was observed after sintering for 10 h, coincident with the increase in Q for the pure PiKem TiO_2. It may be concluded therefore that oxygen deficiency also causes a small decrease in ε_r as well as increasing Q.

From the results discussed above, Q in TiO_2 does not scale with grain size. Instead, sintering for long periods, presumably reoxidising the sample eliminates coring and improves Q. Annealing at lower temperatures (800 °C) marginally improved Q but did not induce the dramatic effect observed by sintering for longer times. In order to investigate further O diffusion in TiO_2 ceramics, secondary ion mass spectroscopy (SIMS) was performed on undoped and Al^{3+} doped samples, but diffusion coefficients for undoped and doped TiO_2 samples were identical within the experimental error. These values are also very close to those reported previously for 0.08 mol% Cr_2O_3 doped TiO_2[23] a material known to exhibit high Q values, and no sign of coring. It was reported that chromium increased the diffusivity of oxygen by between three and eight times. No measurable difference in diffusion rates was observed in this study.

The mechanism responsible for the increase in Q with sintering time in undoped TiO_2 therefore remains unknown. It is not related to grain growth but rather, the defect chemistry appears to be fundamentally different after short sintering times (<10 h) compared with longer. The formation of a core containing $V_O^{\bullet\bullet}$ occurs because Ti^{4+} reduces to Ti^{3+} in air. Since further sintering is also carried out in air, thermodynamically Ti^{3+} should not re-oxidise. Further study is therefore required but it appears that in the early stages of sintering the local effective $P(O_2)$ within the interior is different from the exterior of the pellet in a manner which remains to be elucidated.

3.3. Transmission electron microscopy (TEM) of pure and Al_2O_3 doped titania

Fig. 5 shows TEM images and diffraction patterns from the centre of undoped and Al_2O_3 doped TiO_2. In undoped compositions, grains in the core of the ceramics exhibited a distinct mottled contrast in two beam conditions, shown in low and high magnification in Fig. 5a and b, respectively. In high magnification, it is evident that mottling may be attributed to the presence of planar defects (20 nm) which lie on specific crystallographic planes. In $TiO_{2-\delta}$, it is well known that oxygen

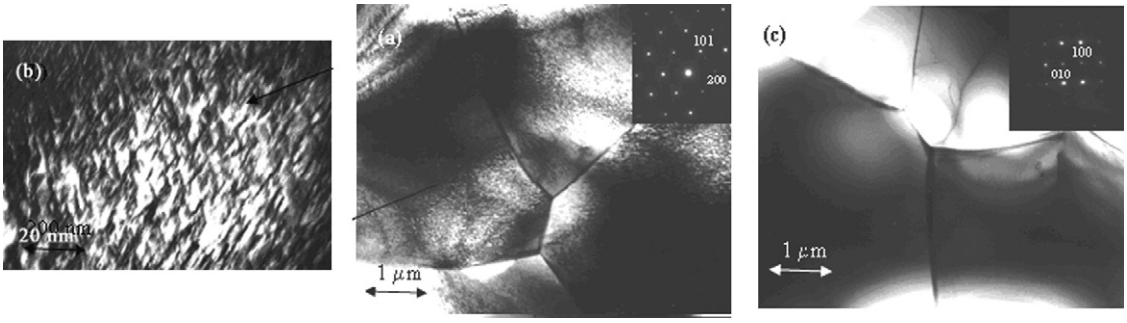

Fig. 5. (a) Bright field (BF) TEM image of the core in undoped TiO_2 showing a mottled underlying strain contrast. Inset is a [0 1 0] zone axis diffraction pattern (ZADP) from the TiO_2 matrix. Strong reflections may indexed according to a rutile structure but weak superlattice reflections are also present at +/−1/3{h 0 1} positions. (b) Two beam dark field (DF) TEM image presenting an enlarged, enhanced view of the planar defects that give rise to the mottled contrast. (c) BF TEM image of Al_2O_3 doped TiO_2 revealing the absence of strain contrast in the image. Inset is a [001] ZADP.

vacancies condense onto specific crystallographic planes which ultimately results in shear planes. The resulting structures are often referred to as Magnelli phases and occur in many simple oxides whose basic structural unit is the octahedron in which resides a multivalent transition metal ion, e.g. WO_3. In TiO_2, processed in air, the bulk oxygen non-stoichiometry is slight, but in the core it may be sufficient to instigate the formation of shear structures/condensation of oxygen vacancies similar to those in Magnelli phases. In the inset diffraction pattern in Fig. 5a, there are extra superlattice reflections at $1/3\{h\,0\,l\}$ positions which result from the presence of the planar defects although their precise mechanism of formation is not clear. In Al^{3+} doped compositions, the mottling is completely absent and no extra reflections were observed in the electron diffraction patterns (Fig. 5c). It is suggested that the presence Al^{3+} has inhibited reduction of Ti^{4+} to Ti^{3+}. This is commensurate with an increase in Q.

4. Conclusions

In high purity, undoped TiO_2 ceramics, sintered at 1400 °C/2 h, high dielectric losses occurred resulting in low Q values, and a dark core was also observed in these samples. Both of these observations were attributed to $V_O^{\bullet\bullet}$ forming at high temperatures, due to the reduction of Ti^{4+} to Ti^{3+}. The formation of O vacancies may be suppressed by doping with 0.05% of metal ions with either 2+ or 3+ valence state, provided the ionic radius is between 0.5 and 0.95 Å. This upper limit proved to be discrete, with almost no effect for dopants $\geq$0.96 Å ionic radius in dense ceramics. A small improvement in Q was also observed for ions with 1+ valence state irrespective of ion size. The Q of undoped TiO_2 could equally be improved by annealing at 1500 °C for >10 h, presumably due to reoxidation of the sample. SEM studies did not reveal any correlation between grain size and Q. TEM of the cores of high and low Q ceramics revealed the presence of a large number of planar defects in the latter, similar to those observed prior to the formation of O-deficient Magnelli phases.

References

1. Grant, F. A., Properties of rutile (titanium dioxide). *Rev. Mod. Phys.*, 1959, **31**, 646–674.
2. Harrison, W. H., A miniature high-*Q* bandpass filter employing dielectric resonators. *IEEE Trans. MTT*, 1968, **16**, 210–218.
3. Cohn, S. B., Microwave bandpass filters containing high-*Q* dielectric resonators. *IEEE Trans. MTT*, 1968, **16**, 218–227.
4. Negas, T., Yeager, G., Bell, S., Coats, N. and Minis, I., $BaTi_4O_9/Ba_2Ti_9O_{20}$-based ceramics resurrected for modern microwave applications. *Am. Ceram. Soc. Bull.*, 1993, **72**, 80–89.
5. Nomura, S., Tomaya, K. and Kaneta, K., Effect of Mn doping on the dielectric properties of $Ba_2Ti_9O_{20}$ ceramics at microwave frequencies. *Jpn. J. Appl. Phys.*, 1983, **22**, 1125–1128.
6. Cheary, R. W. and Dryden, J. S., Dielectric relaxation in hollandites and rutile. *Phil. Mag. B*, 1991, **64**, 709–722.
7. Reece, M. and Morrell, R., Electron microscope study of non-stoichiometric titania. *J. Mater. Sci.*, 1991, **26**, 5566–5574.
8. Ikeda, J. A. S., Chiang, Y. M., Garratt-Reed, A. J. and Vander Sande, J. B., Space charge segregation at grain boundaries in titanium dioxide. II. Model experiments. *J. Am. Ceram. Soc.*, 1993, **76**, 2447.
9. Templeton, A., Wang, X., Penn, S. J., Webb, S. J., Cohen, L. F. and Alford, N. McN., Microwave dielectric loss of titanium oxide. *J. Am. Ceram. Soc.*, 2000, **83**, 95–100.
10. Crossland, I. G. and Clay, D. D., Diffusion creep and its inhibition in a strainless steel. *Acta Met.*, 1977, **25**, 929.
11. Kajfez, D. P., *Guillon in Dielectric Resonators* (*2nd ed.*). Noble Publishing Corp., Georgia, USA, 1998, pp. 327–377.
12. Wakino, K., Recent development of dielectric resonator materials and filters in Japan. *Ferroelectrics*, 1989, **91**, 69–86.
13. Shannon, R. D., Revised effective ionic radii and systematic studies of interatomic distances in halides and chalcogenides. *Acta Crystallogr.*, 1976, **A32**, 751.
14. Kroger, F. A., *Physical Chemistry: An Advanced Treatise*, *vol. X*. Academic Press, New York, USA, 1970, pp. 229–259.
15. Eror, N. G., Self-compensation in niobium-doped TiO_2. *J. Solid State Chem.*, 1981, **38**, 281–287.
16. Balachandran, U. and Eror, N. G., Self-compensation in tantalum-doped TiO_2. *J. Mater. Sci.*, 1982, **17**, 1207–1212.
17. Chiang, Y.-M., Birnie, D. and Kingery, W. D., *Physical Ceramics: Principles for Ceramic Science and Engineering*. Wiley, New York, USA, 1997.
18. Holgado, J. P., Munuera, G., Espinós, J. P. and González-Elipe, A. R., XPS study of oxidation processes of CeO_x defective layers. *Appl. Surf. Sci.*, 2000, **158**, 164–171.
19. Kümmerle, E. A. and Heger, G., The structures of C–$Ce_2O_{3+\delta}$, Ce_7O_{12}, and $Ce_{11}O_{20}$. *J. Solid State Chem.*, 1999, **147**, 485–500.
20. Molycorp data sheet 5500 for Praseodymium Oxide.
21. Wolffframm, D., Ratzke, M., Kappa, M., Montenegro, M. J., Dobeli, M., Lippert, Th. and Reif, J., Pulsed laser deposistion of thin film PrxOy films on Si(100). In *Presented at EMRS Spring Meeting*, 2003.
22. Penn, S. J., Alford, N. McN., Templeton, A., Wang, X., Xu, M., Reece, M. and Schrapel, K., Effect of porosity and grain size on the microwave dielectric properties of sintered alumina. *J. Am. Ceram. Soc.*, 1997, **80**, 1885–1888.
23. Arita, M., Hosoya, M., Koyashi, M. and Someno, M., Depth profile measurement by secondary ion mass spectrometry for determining the tracer diffusivity of oxygen in rutile. *J. Am. Ceram. Soc.*, 1979, **62**, 443.